Journal of Glaciology, Vol. 34, No. 116, 1988

ICE-SHELF RESPONSE TO ICE-STREAM DISCHARGE FLUCTUATIONS: I. UNCONFINED ICE TONGUES

By DOUGLAS R. MACAYEAL *and* VICTOR BARCILON

(Department of Geophysical Sciences, University of Chicago, Chicago, Illinois 60637, U.S.A.)

ABSTRACT. Ice-stream discharge fluctuations constitute an independent means of forcing unsteady ice-shelf behavior, and their effect must be distinguished from those of oceanic and atmospheric climate to understand ice-shelf change. In addition, ice-stream-generated thickness anomalies may constitute a primary trigger of ice-rise formation in the absence of major sea-level fluctuations. Such triggering may maintain the current ice-rise population that, in turn, contributes to long-term ice-sheet stability. Here, we show that ice-stream-generated fluctuations of an ideal, two-dimensional ice shelf propagate along two characteristic trajectories. One trajectory permits instantaneous transmission of grounding-line velocity changes to all points down-stream. The other trajectory represents slow transmission of grounding-line thickness changes along Lagrangian particle paths.

INTRODUCTION

Unsteady thickness and flow observed on the Ross Ice Shelf result primarily from fluctuations of ice streams and outlet glaciers that feed the ice shelf at its inland boundaries (MacAyeal and others, 1987; Shabtaie and Bentley, 1987). Investigations of climatic evolution therefore must discriminate atmospheric and oceanic effects from ever-present background of ice-stream-generated variability. Ice-stream forcing additionally may produce thickness fluctuations in sensitive areas where the sub-ice-shelf water column is shallow. Ice-shelf grounding triggered in this way could damp anomalous ice-stream acceleration, and thus provide a stabilizing feed-back on ice-stream fluctuations driven by other physical processes.

In this study, we determine the general patterns of ice-thickness and flow anomalies produced by time-varying grounding-line discharge. Our examination is restricted to anomalies of an ideal, floating ice tongue to facilitate an analytic treatment of the hyperbolic governing equations. This treatment suggests that two distinct characteristic trajectories constitute an underlying organization to seemingly disjoint ice-stream forcing events. This organization provides: (i) a conceptual basis for modelling thickness and flow variations of West Antarctic ice shelves (such as developed in a companion paper; MacAyeal and Lange, 1988), and (ii) an understanding of how inland-ice discharge may compete with oceanic and atmospheric conditions to force such variations.

CHARACTERISTIC EQUATIONS

As shown in the Appendix (see also Morland, 1987; Morland and Zainuddin, 1987), large-scale horizontal flow of typical Antarctic ice shelves is essentially depth independent. We thus treat thickness $H(x,t)$ and longitudinal velocity $U(x,t)$ of the ideal, two-dimensional ice shelf considered here (Fig. 1) in a manner consistent with this simplification. Time evolution of H and U is governed by

$$\partial_t H + U\partial_x H = M - A^n H^{n+1}, \quad x > 0, \tag{1}$$

$$\partial_x U = A^n H^n, \quad x > 0 \tag{2}$$

by grounding-line boundary conditions

$$H(0,t) = H_g(t), \quad x = 0, \tag{3}$$

$$U(0,t) = U_g(t), \quad x = 0 \tag{4}$$

where U_g is the depth-averaged horizontal velocity at the grounding line (see Appendix), and by the initial condition

$$H(x,0) = H_i(x) \quad x > 0. \tag{5}$$

Dimensionless variables are defined in Table I and are scaled using typical dimensions of Antarctic ice tongues (Holdsworth, 1985).

Equations (1)–(5) are derived in the Appendix and represent mass-continuity and stress-equilibrium constraints that have been simplified to exploit the small aspect ratio δ (ratio of thickness to horizontal span) of the large-scale features considered here. Ice rheology is treated by a simple power-law relationship between the strain-rate and the deviatoric stress (in the Appendix, a strain-rate dependent effective viscosity is defined). Additional simplifications include: (i) all variables are independent of the horizontal direction transverse to the flow, (ii) resistance to seaward flow is provided by sea-water pressure only, and (iii) the snow-accumulation rate M is constant in space and time. Our ideal ice shelf behaves, in effect, as if it were confined in a narrow but frictionless channel.

As shown in the Appendix, Equations (1)–(5) do not describe flow structure possessing large vertical gradients. Such deviations from the simple large-scale flow, however, can persist only short horizontal distances. We hence-henceforth disregard such structure in our examination of

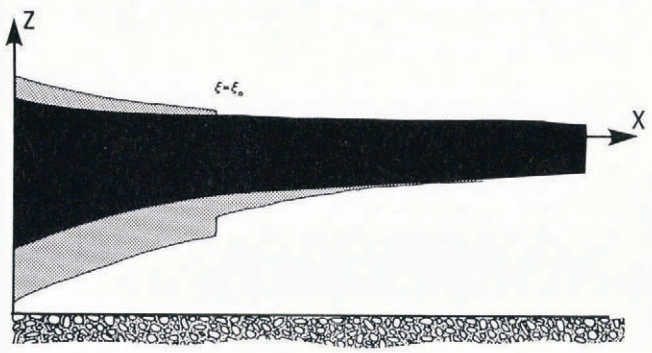

Fig. 1. Cross-section of ideal ice shelf considered in this study. The trajectory of the ice column labeled ξ_0 follows one of the two types of characteristics associated with the governing equations. If ice-stream discharge was impulsively changed between two otherwise steady conditions at the time this ice column was at the grounding line, the subsequent locations of this ice column will separate the region where steady-state conditions have been renewed (up-stream) from the region where adjustment is still under way (down-stream).

https://doi.org/10.3189/S002214300000914X Published online by Cambridge University Press

TABLE I. VARIABLES AND SCALES

Variable	Definition	Units	Scales	
			Symbol	Value
H	Ice thickness	m	H_0	10^3
U	Horizontal velocity	m/s	U_0	1.58×10^{-5}
h	Thickness anomaly	m	H_0	10^3
u	Velocity anomaly	m/s	U_0	1.58×10^{-5}
u_n, u_f	Near- and far-field horizontal velocity	m/s	U_0	1.58×10^{-5}
w_n, w_f	Near- and far-field vertical velocity	m/s	U_0	1.58×10^{-5}
ξ	Characteristic coordinate	m	L_0	10^4
τ	Characteristic coordinate	s	L_0/U_0	6.33×10^8
x	Horizontal coordinate	m	L_0	10^4
z	Vertical coordinate	m	H_0	10^3
δ	Aspect ratio	-	H_0/L_0	10^{-1}
t	Time	s	L_0/U_0	6.33×10^8
M	Accumulation rate	m/s	U_0H_0/L_0	7.92×10^{-9}
ρ_i	Ice density	kg/m^3	ρ_i	917
g	Gravity	m/s^2	g	9.81
ρ_w	Sea-water density	kg/m^3	ρ_w	1028
B	Flow-law constant	Pa s$^{-1/n}$	B_0	1.5×10^8
n	Flow-law exponent		3	
A	Stress ratio		$\dfrac{\rho g H_0(1 - \rho_i/\rho_w)}{4(U_0/L_0)^{1/n}B_0}$	1.39
p	Pressure	Pa	$\rho_i g H_0$	9.0×10^6
e_{xx}	Longitudinal strain-rate	s^{-1}	U_0/L_0	1.58×10^{-9}
e_{zz}	Vertical strain-rate	s^{-1}	U_0/L_0	1.58×10^{-9}
e_{xz}	Vertical shear-rate	s^{-1}	$\delta^{-1}U_0/L_0$	1.58×10^{-8}
υ	Effective viscosity	Pa s	$B_0/\{2(U_0/L_0)^{1-1/n}\}$	5.5×10^{13}
T'_{ij}	Deviatoric stress	Pa	$\rho_i g H_0$	9.0×10^6
z_s	Surface elevation	m	H_0	10^3
z_b	Basal depth	m	H_0	10^3
Γ	Stress ratio	Non-dimensional	$\rho_i g H_0/\{B_0(U_0/L_0)^{1/n}\}$	51.4

large-scale ice-shelf behaviour. In demonstrating properties of Equations (1)–(5), for example, we shall consider the response to a step-like thickness jump introduced at the ice-stream outlet. Strictly speaking, this type of forcing violates one of the assumptions underlying the derivation of Equations (1)–(5), namely that gradients of thickness are small. Nevertheless, this forcing is adopted because it generates the impulse response for the problem; and it gives rise to a flow which illustrates simply and vividly the features of all responses.

STEADY-STATE SOLUTIONS

Steady-state solutions of Equations (1)–(5), $H_s(x)$ and $U_s(x)$, satisfying $H_s(0) = 1$ and $U_s(0) = 1$ at the grounding line were found by van der Veen (1983) and are written (for $M > 0$):

$$H_s(x) = [(1 - \gamma)/(1 + Mx)^{n+1} + \gamma]^{(-1/(n+1))}, \quad (6)$$

$$U_s(x) = [1 - \gamma + \gamma(1 + Mx)^{n+1}]^{(1/(n+1))} \quad (7)$$

where $\gamma = A^n/M$. $H_s(x)$ monotonically decreases with increasing distance from the grounding line and approaches a constant value $\gamma^{-1/(n+1)}$ as $x \to \infty$. This asymptotic thickness (approximately 200 m for typical Antarctic conditions) is achieved because ice-shelf thinning by horizontal spreading is balanced by snow accumulation M. $U_s(x)$ monotonically increases with distance from the grounding line, but does not approach an asymptotic limit as $x \to \infty$.

CHARACTERISTIC EQUATIONS

Deviations from steady state caused by fluctuations in H and U at the grounding line can be computed directly from Equations (1) and (2). Alternative forms of Equations (1) and (2), called the characteristic equations, are useful, however, for displaying fundamental properties of the solution. They are derived by defining new spatial and temporal coordinates that produce ordinary differential equations for thickness and velocity (the method of characteristics) and are written as:

$$\partial_\tau x - \hat{U}\partial_\tau t = 0, \quad (8)$$

$$\partial_\xi t = 0, \quad (9)$$

$$\partial_\tau \hat{H} - (M - A^n\hat{H}^{n+1})\partial_\tau t = 0, \quad (10)$$

$$\partial_\xi \hat{U} - A^n \hat{H}^n \partial_\xi x = 0 \quad (11)$$

where $\hat{H}(\xi,\tau)$ and $\hat{U}(\xi,\tau)$ represent thickness and velocity, respectively, as functions of alternative coordinates ξ and τ that satisfy

$$\partial_t \xi + \hat{U}\partial_x \xi = 0, \quad (12)$$

$$\partial_x \tau = 0. \quad (13)$$

The curves $\xi = \xi_0$ and $\tau = \tau_0$ in the x,t plane represent characteristics of the ice-shelf system along which changing conditions propagate. These curves can be determined by solving Equations (8) and (9) for $x(\xi,\tau)$ and $t(\tau)$ (t and τ

https://doi.org/10.3189/S002214300000914X Published online by Cambridge University Press

can be taken as identical in the present application; this gives $\partial_\tau t = 1$).

As shown by Equation (12), the characteristic $\xi = \xi_0$ represents the trajectory of a particular ice column (which may be labeled by its ξ-coordinate ξ_0) in the x,t plane. The thickness of this particular ice column, $\hat{H}(\xi = \xi_0,\tau)$, is determined as a function of τ by Equation (10). The velocity of this ice column, $\hat{U}(\xi = \xi_0,\tau)$, is found by integrating Equation (11) over the domain $\xi_1(\tau) < \xi < \xi_0$ where $\xi_1(\tau)$ is the ξ-label of the ice column currently at the grounding line. This interval, in x-coordinates, spans the distance between the grounding line and $x = x(\xi_0,\tau)$.

The characteristic equations illuminate several basic aspects of time-dependent ice-shelf adjustment. Equation (10) indicates that the thickness of a given ice column (ξ = constant) evolves independently of the ice thickness elsewhere. This independence is an aspect of unconfined ice shelves only. In circumstances where coastal confinement introduces resistance to seaward flow, evolution of a given ice column depends on thickness conditions down-stream.

Another basic aspect of ice-shelf behavior illuminated by Equations (10) and (11) is that deviations from steady-state are limited in space and time by the appropriate characteristic curves. If, for example, H or U at $x = 0$ are impulsively changed at $t = 0$ and the initial conditions are in steady state; unsteady conditions will prevail only within the region of the x,t plane bounded by the curves ξ = constant and τ = constant that emanate from $x = t = 0$. This partition of the x,t plane into steady and unsteady regions is shown schematically in Figure 2. Change

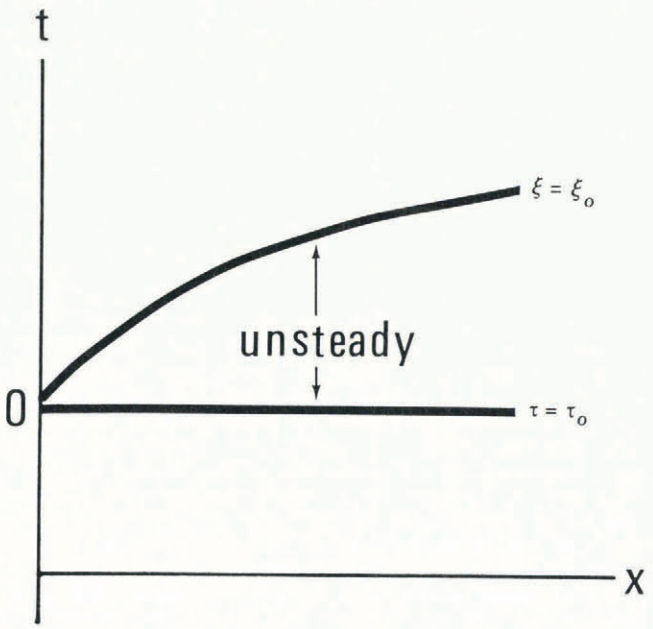

Fig. 2. If ice-stream discharge (grounding-line thickness and velocity) is changed impulsively at $t = 0$, unsteady conditions will prevail only within the region of the x,t plane bounded by the ξ = constant and τ = constant characteristics.

propagates down-stream instantaneously along the τ = constant curve because velocity at any point is determined by spatial integration of the instantaneous ice-thickness distribution. Equilibration with new forcing conditions is completed, however, in a delayed fashion following the ξ = constant curve. Steady-state conditions prevail in the wake of the ice column that was at the grounding line at the instant $t = 0$. This ice column follows the path determined by the ξ = constant characteristic.

TRANSIENT ICE-SHELF PROFILES

We demonstrate basic ice-shelf response by computing ice-thickness and velocity anomalies generated by prescribed scenarios of unsteady grounding-line discharge. These anomalies are defined by

$$h(x,t) = H(x,t) - H_S(x), \tag{14}$$

$$u(x,t) = U(x,t) - U_S(x) \tag{15}$$

where $H_S(x)$ and $U_S(x)$ are the steady-state thickness and velocity profiles defined by Equations (6) and (7) respectively. To simplify the calculations, we require h and u to be small and use a linear expansion of Equations (1) and (2):

$$\partial_t h + U_S \partial_x h = -(n+1)A^n H_S{}^n h - \partial_x H_S u, \tag{16}$$

$$\partial_x u = nA^n H_S{}^{n-1} h. \tag{17}$$

With this simplification, the two generic characteristic curves ξ = constant and τ = constant associated with steady-state conditions may be applied as approximations to the characteristic curves associated with unsteady conditions.

Boundary conditions at the grounding line ($x = 0$) and initial conditions are specified to represent three basic scenarios of ice-stream discharge fluctuations (amplitudes and time constants are arbitrary for demonstration):

scenario I — $u(x,0) = h(x,0) = 0.0$, (18)

$$u(0,t) = h(0,t) = 0.1,\ 0 \to t \to 0.2,$$

$$0.0,\ t > 0.2$$

scenario II — $h(0,t) = 0.1\sin(\omega t)$, (19)

$$u(0,t) = 0.0$$

scenario III — $h(0,t) = 0.0$, (20)

$$u(0,t) = 0.1\sin(\omega t)$$

where $\omega = 2\pi/0.5$. Scenario I represents an episode of increased grounding-line thickness and velocity that is sustained for a brief time interval. Scenarios II and III represent periodic fluctuations in h and u (we do not consider a variety of forcing frequencies in the present study; see, however, MacAyeal and Lange, 1988). Initial conditions for scenarios II and III are not required because the grounding-line forcing is assumed to proceed *ad infinitum* (in practice, we apply an initial condition of $h(x,0) = 0$ and $u(x,0) = 0$, and proceed with time integration until all manifestations of the initial conditions have dissipated).

For demonstration purposes, finite-difference solutions to Equations (16) and (17) under the three forcing scenarios described above were produced on the interval $0 \leqslant x \leqslant 1$ and over a sufficient time interval to display salient features (and to dissipate transients induced by initial conditions in periodic forcing scenarios). The finite-difference form of Equation (16) possessed fully implicit time steps ($\Delta t = 0.01$) and centered space derivatives ($\Delta x = 0.01$), except at $x = 1.0$ where an up-wind space derivative was used. Equation (17) was integrated over x at each time step using centered space derivatives (except up-wind at $x = 1.0$). This crude finite-difference method is notorious for introducing artificial smoothing and dispersion in hyperbolic systems (a more refined technique was not considered necessary for demonstration purposes). The results described below, nevertheless, demonstrate that the strong underlying organization provided by the characteristic curves persists even in crude finite-difference solutions.

Salient features of scenario I are displayed by the contour maps of thickness anomaly h and volume-flux anomaly q, defined by

$$q(x,t) = u(x,t)H_S(x) + h(x,t)U_S(x) \tag{21}$$

https://doi.org/10.3189/S002214300000914X Published online by Cambridge University Press

in Figure 3. In Figure 4, the x,t plane on which these maps are presented is divided into five regions by the four characteristic curves that emanate from the grounding line at the start and end of the modified discharge episode. In regions I, III, and V shown in Figure 3, ice-shelf conditions are in steady state with current discharge thickness and velocity ($H_S(0) + h(0,t)$, and $U_S(0) + u(0,t)$). In regions II and IV, conditions are unsteady. Comparison of the maps of h and q indicates that thickness anomalies are organized primarily along ξ = constant trajectories and that flux anomalies tend to display rapid, discontinuous changes across τ = constant trajectories.

Ice-thickness anomalies generated in response to scenarios II and III (periodic forcing) indicate two contrasting patterns shown in Figure 5. For oscillatory grouding-line thickness (scenario II), h is maximum at the grounding line, and decays monotonically down-stream. Ridges and troughs of the $h(x,t)$ contours in the x,t plane extend along ξ = constant trajectories. In contrast, the maximum of h generated by scenario III (oscillatory grounding-line velocity) is smaller than in scenario II and occurs down-stream of the grounding line. The down-stream maximum of h results from velocity anomalies at locations where the gradient of $H_S(x)$ is large. In addition, the $h(x = 0) = 0$ constraint demands that the maximum of h be separated from the ice-stream outlet.

Comparison of scenarios II and III suggests that phase relationships between thickness and velocity oscillations of a given ice stream is critical in determining the location of maximum ice-thickness anomalies. This aspect of ice-stream dynamics may thus determine where ice rumples and ice rises are likely to form in response to ice-stream acceleration.

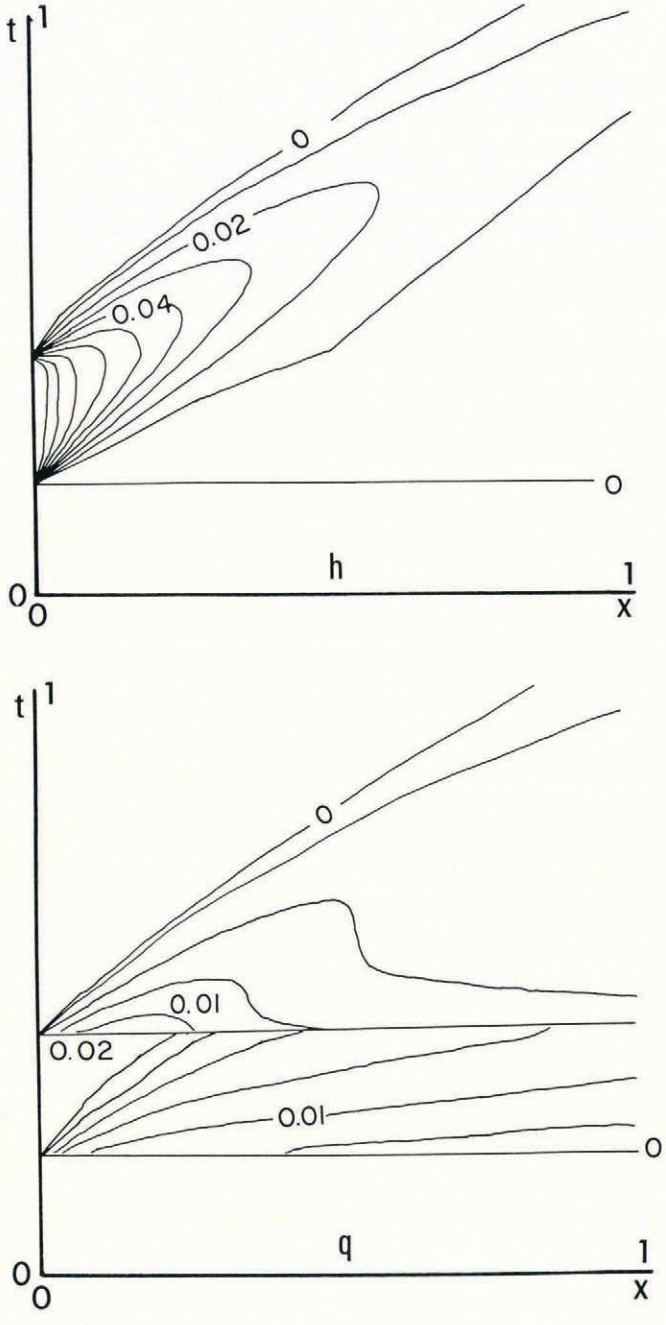

Fig. 3. Ice-thickness (top) and flux (bottom) anomalies (non-dimensional units; Table I) resulting from a limited episode of modified ice-stream discharge (scenario I). The ranges of x and t displayed above are both 0.0 → 1.0 (non-dimensional units). Comparison with the characteristics shown in Figure 4 suggests that thickness anomalies primarily follow ξ = constant characteristics, whereas flux anomalies primarily follow τ = constant characteristics.

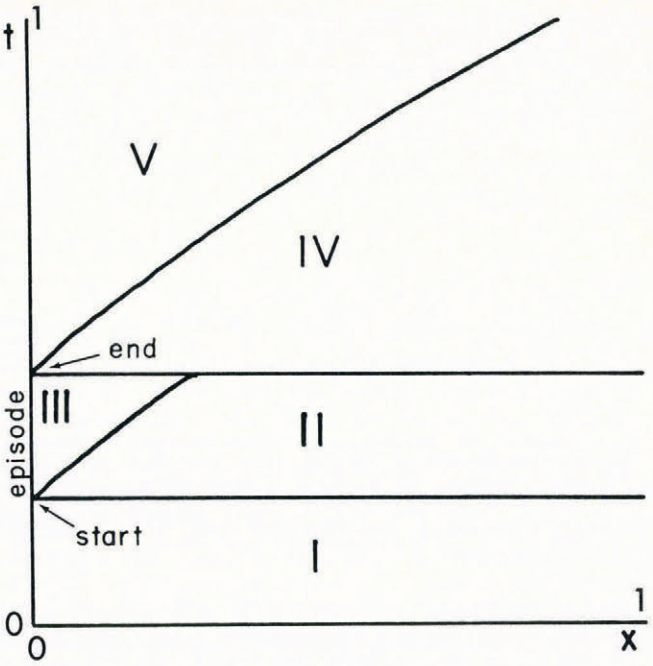

Fig. 4. Ice-shelf response can be organized in terms of steady and unsteady behavior using the ξ- and τ-characteristics to partition the x,t plane. In scenario I, for example, the x,t plane is divided into five regions by the four characteristics that emanate from x = 0 at the start and end of the ice-stream discharge episode. Regions I, III, and V are in steady state with current ice-stream discharge (for region III, this discharge is greater than for regions I and V); regions II and IV display unsteady conditions.

CONCLUSION

Discrimination between ice-stream forcing and climatic forcing in the ideal, two-dimensional ice shelf can be accomplished through the relationship between ice-shelf anomalies and the characteristic trajectories that determine propagation of ice-shelf change. Variability forced by the atmosphere or ocean would not necessarily be constrained by such trajectories, but may propagate through the ice-shelf environment along pathways determined by oceanic and atmospheric dynamics.

While only very simple ice-shelf geometries are amenable to treatment using the method of characteristics, qualitative aspects of ice-shelf behavior demonstrated here are expected in more complex, natural geometries where coastal confinement plays a larger role. The two types of characteristics described here, for example, represent fast and slow paths by which grounding-line influences are

https://doi.org/10.3189/S002214300000914X Published online by Cambridge University Press

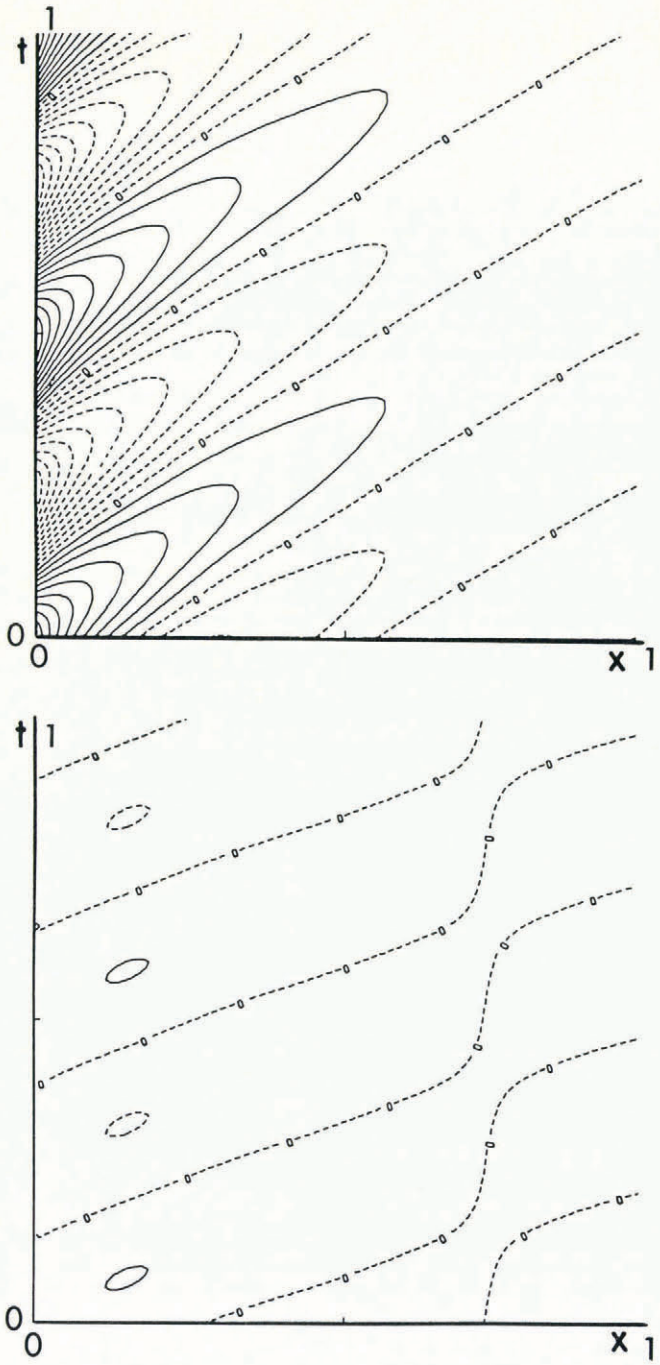

Fig. 5. Ice-thickness anomalies driven by periodic fluctuations in ice-stream thickness (top, scenario II) and velocity (bottom, scenario III). Contour intervals are 0.01 non-dimensional units, negative values are contoured with dashed pattern. The ranges of x and t displayed are both 0.0 → 1.0. Note that maximum h for scenario III occurs down-stream of the grounding line.

transmitted to the ice shelf down-stream. In natural ice-shelf geometries, velocity and mass-flux changes are expected to propagate via an analogous fast path because the velocity profile is determined by an elliptic boundary-value operator. Thickness changes, in contrast, are expected to propagate via an analogous slow path because ice thickness evolves primarily by ice-column advection.

ACKNOWLEDGEMENTS

This research was supported by the U.S. National Science Foundation (DPP 85 09451) and the U.S. Office of Naval Research under grant N00014-86-K-0034. We thank L.W. Morland for productive discussions at the University of Chicago in December 1986.

REFERENCES

Barcilon, V. 1967. On the motion due to sources and sinks distributed along the vertical boundary of a rotating fluid. *Journal of Fluid Mechanics*, 27(3), 551-60.

Bindschadler, R.A., Stephenson, S.N., MacAyeal, D.R., *and* Shabtaie, S. 1987. Ice dynamics at the mouth of Ice Stream B, Antarctica. *Journal of Geophysical Research*, 92(B9), 8885-94.

Herterich, K. 1987. On the flow within the transition zone between ice sheet and ice shelf. *In* Veen, C.J. van der, *and* Oerlemans, J., *eds. Dynamics of the West Antarctic Ice Sheet. Proceedings of a Workshop held in Utrecht, May 6–8, 1985.* Dordrecht, D. Reidel Publishing Company, 185-202.

Holdsworth, G. 1985. Some effects of ocean currents and wave motion on the dynamics of floating glacier tongues. *In* Jacobs, S.S., *ed. Oceanology of the Antarctic continental shelf.* Washington, DC, American Geophysical Union, 253-71. (Antarctic Research Series, **43**.)

Hutter, K. 1983. *Theoretical glaciology; material science of ice and the mechanism of glaciers and ice sheets.* Dordrecht, etc., D. Reidel Publishing Company/Tokyo, Terra Scientific Publishing Company.

MacAyeal, D.R., *and* Lange, M.A. 1988. Ice-shelf response to ice-stream discharge fluctuations: II. Ideal rectangular ice shelf. *Journal of Glaciology*, **34**(116), 128-35.

MacAyeal, D.R., Bindschadler, R.A., Shabtaie, S., Stephenson, S., *and* Bentley, C.R. 1987. Force, mass, and energy budgets of the Crary Ice Rise complex, Antarctica. *Journal of Glaciology*, **33**(114), 218-30.

Morland, L.W. 1987. Unconfined ice-shelf flow. *In* Veen, C.J. van der, *and* Oerlemans, J., *eds. Dynamics of the West Antarctic Ice Sheet. Proceedings of a Workshop held in Utrecht, May 6–8, 1985.* Dordrecht, D. Reidel Publishing Company, 99-116.

Morland, L.W., *and* Shoemaker, E.M. 1981. Ice shelf balances. *Cold Regions Science and Technology*, 5(3), 235-51.

Morland, L.W., *and* Zainuddin, R. 1987. Plane and radial ice-shelf flow with prescribed temperature profile. *In* Veen, C.J. van der, *and* Oerlemans, J., *eds. Dynamics of the West Antarctic Ice Sheet. Proceedings of a Workshop held in Utrecht, May 6–8, 1985.* Dordrecht, D. Reidel Publishing Company, 117-40.

Muszynski, I., *and* Birchfield, G.E. 1987. A coupled marine ice-stream–ice-shelf model. *Journal of Glaciology*, **33**(113), 3-15.

Sanderson, T.J.O., *and* Doake, C.S.M. 1979. Is vertical shear in an ice shelf negligible? *Journal of Glaciology*, 22(87), 285-92.

Shabtaie, S., *and* Bentley, C.R. 1987. West Antarctic ice streams draining into the Ross Ice Shelf: configurations and mass balance. *Journal of Geophysical Research*, **92**(B2), 1311-36.

Shumskiy, P.A., *and* Krass, M.S. 1976. Mathematical models of ice shelves. *Journal of Glaciology*, **17**(77), 419-32.

Veen, C.J. van der. 1983. A note on the equilibrium profile of a free floating ice shelf. *Rijksuniversiteit, Utrecht. Instituut voor Meteorologie en Oceanografie. Technical Report*, **83**(15).

Williams, F.M., *and* Hutter, K. 1983. Thermal response of unconfined ice shelves to climatic conditions. *Acta Mechanica*, **48**, 131-46.

Yih, C.-S. 1969. *Fluid mechanics.* New York, McGraw-Hill.

APPENDIX

DERIVATION OF GOVERNING EQUATIONS

Ice shelves float in a relatively inviscid environment and span horizontal dimensions that greatly exceed the maximum ice thickness. These physical characteristics imply that large-scale ice-shelf flow is relatively simple. In particular, vertical shear is negligible, and relatively weak vertical velocity exists only to maintain the surface and basal elevations in local hydrostatic balance (Sanderson and Doake, 1979; Morland, 1987; Muszynski and Birchfield, 1987). In spite of its simplicity, large-scale ice-shelf flow is

https://doi.org/10.3189/S002214300000914X Published online by Cambridge University Press

forced by ice-stream influx, ice-front pressure balances, and lateral shears that can be arbitrarily complex. Ice-shelf dynamics in the neighborhood of such lateral boundaries, therefore, must winnow flow structure that is incompatible with large-scale flow. In the following analysis, we describe this winnowing process and derive Equations (1)–(5) that are used to investigate large-scale ice-shelf behavior.

To facilitate our derivation, we express the ice-shelf velocity and pressure fields as the sums of far-field and near-field contributions (denoted by the subscripts f and n, respectively):

$$u = u_f(x,z) + u_n(\zeta,z), \tag{A1}$$

$$w = \delta w_f(x,z) + w_n(\zeta,z), \tag{A2}$$

$$p = p_f(x,z) + p_n(\zeta,z). \tag{A3}$$

The far-field contributions describe the simple, large-scale flow that dominates the ice-shelf interior (locations remote from lateral boundaries). The near-field contributions are corrections needed to satisfy boundary conditions at the ice-stream outlet (or at other lateral boundaries).

The separation between far-field and near-field contributions is accomplished by defining two dependent coordinates, x and $\zeta = \delta^{-1}x$, that express horizontal distance along the same longitudinal axis. The coordinate x is scaled by the horizontal span of the ice shelf L_0. This span is typically much greater than the characteristic vertical scale H_0; thus x becomes order one in size at points far removed from the grounding line. The coordinate ζ is scaled by the characteristic vertical scale of the ice shelf H_0, and thus grows rapidly within a short distance of the grounding line $x = \zeta = 0$.

Ideally, the goal of the following analysis should be to show that the near-field and far-field contributions can be made to match asymptotically as $\zeta \to \infty$ and $x \to 0$, respectively. If this goal were met, the far-field contribution alone would represent large-scale flow. The asymptotic limit of the near-field contribution, in this circumstance, would simply provide the suitably winnowed lateral boundary condition on the far-field flow. This winnowed boundary condition would be simpler than that actually imposed by the ice stream, and thus would be compatible with large-scale dynamics.

We shall fall short of this goal and succeed only in deriving the far-field equations. The near-field winnowing process is too complex to demonstrate its asymptotic limits under the most general circumstances. We proceed to demonstrate the winnowing process, however, under more restrictive, yet physically motivated simplifications. In particular, we linearize the near-field stress-equilibrium equations by replacing the stress-dependent effective viscosity (defined below) with a constant. This simplification permits exact solution for eigenfunctions with which the most general ice-stream forcing can be described. The constant viscosity we apply, however, need not be associated with any specific reference stress (e.g. the far-field stress, the near-field stress, or some combination of the two). Observations suggest, however, that near-field contributions are minor, in an absolute sense, because typical ice-stream flow can be similar to far-field ice-shelf flow if basal shear stress is sufficiently low (Muszynski and Birchfield, 1987). In this circumstance, the linearization of the near-field equations can be made using the far-field stress as a reference state.

The upper and lower surfaces of the ice shelf, $z_s(x)$ and $z_b(x)$, are assumed to be functions of the far-field coordinate x only. This assumption is compatible with observations that suggest surface and basal topography at the grounding line is not abrupt (Bindschadler and others, 1987). In some demonstrations of large-scale behavior, we introduce step-like changes in surface and basal topography at the grounding line. This violates the above assumption insofar as we do not specify the small-scale behavior that would surround such steps. For the purpose of our demonstrations, however, it is sufficient to realize that large-scale flow can bridge such step-like topography (or any topography organized on the scale of H_0 or smaller) in a manner analogous to the near-field boundary layer described below. We additionally assume a state of local hydrostatic equilibrium between the surface and basal elevations at the grounding line $x = \zeta = 0$, $z_b = -(\rho_i/\rho_w)(z_s - z_b)$. Observations suggest the location of the grounding line, in fact, is determined by this condition (Bindschadler and others, 1987).

Several other simplifications beyond those motivated by natural ice-shelf configuration are applied here to facilitate an analytic treatment. First, temperature-dependent rheological parameters are replaced with similar depth-dependent parameters to approximate the prevalent vertical temperature gradient in Antarctic ice shelves. Thermo-mechanical coupling (as by, Shumskiy and Krass, 1979; Morland and Shoemaker, 1981; Williams and Hutter, 1983) is not a subject of our study. Secondly, we restrict our analysis to the ideal two-dimensional ice tongue shown in Figure 1. As stated previously, our third, and most grave simplification concerns the treatment of ice rheology in near-field dynamics.

FAR-FIELD DYNAMICS

Stress equilibrium in the far-field horizontal (x) and vertical (z) directions, and dynamic boundary conditions at the ice-shelf surface ($z_s(x)$, stress-free) and base ($z_b(x)$, sea-water pressure only), are written in terms of far-field variables only (subscripts f are dropped for clarity):

$$-\Gamma\partial_x P + \partial_x(\upsilon e_{xx}) + \delta^{-2}\partial_z(\upsilon e_{xz}) = 0, \quad z_b < z < z_s, \tag{A4}$$

$$-\Gamma\partial_z P + \partial_x(\upsilon e_{xz}) + \partial_z(\upsilon e_{zz}) - \Gamma = 0, \quad z_b < z < z_s, \tag{A5}$$

$$-\partial_x z_s(\upsilon e_{xx} - \Gamma P) + \delta^{-2}\upsilon e_{xz} = 0, \quad z = z_s, \tag{A6}$$

$$-\partial_x z_s \upsilon e_{xz} + \upsilon e_{zz} - \Gamma P = 0, \quad z = z_s, \tag{A7}$$

$$\partial_x z_b(\upsilon e_{xx} - \Gamma P) - \delta^{-2}\upsilon e_{xz} = (\rho_w/\rho_i)\Gamma\partial_x(\tfrac{1}{2}z_b^2), \quad z = z_b, \tag{A8}$$

$$\partial_x z_b \upsilon e_{xz} - \upsilon e_{zz} + \Gamma P = -(\rho_w/\rho_i)\Gamma z_b, \quad z = z_b. \tag{A9}$$

A viscous flow law

$$T_{ij}' = 2\upsilon e_{ij} \tag{A10}$$

where effective viscosity υ is

$$\upsilon = B(z)/[(\tfrac{1}{2}(e_{xx}^2 + e_{zz}^2 + 2e_{xz}^2))^{\frac{1}{2}-1/(2n)}] \tag{A11}$$

is defined to represent Glen's flow law. As stated above, the non-dimensional flow-law parameter $B(z)$ is assumed z-dependent, rather than temperature-dependent, to avoid thermo-mechanical coupling.

Systematic approximations to Equations (A4)–(A9) are developed by expanding all variables in power series using the small parameter δ^2. The zero-order approximations to Equations (A4)–(A9) constitute the ice-shelf equivalent to the shallow-ice approximation describing lead-order ice-sheet dynamics (Hutter, 1983) and are written:

$$\partial_z(\upsilon^{(0)}e_{xz}^{(0)}) = 0, \quad z_b^{(0)} < z < z_s^{(0)}, \tag{A12}$$

$$-\Gamma\partial_z P^{(0)} + \partial_x(\upsilon^{(0)}e_{xz}^{(0)}) + \partial_z(\upsilon^{(0)}e_{zz}^{(0)}) - \Gamma = 0, \quad z_b^{(0)} < z < z_s^{(0)}, \tag{A13}$$

$$\upsilon^{(0)}e_{xz}^{(0)} = 0, \quad z = z_s^{(0)}, \tag{A14}$$

$$-\partial_x z_s^{(0)}\upsilon^{(0)}e_{xz}^{(0)} + \upsilon^{(0)}e_{zz}^{(0)} - \Gamma P^{(0)} = 0, \quad z = z_s^{(0)}, \tag{A15}$$

$$\upsilon^{(0)}e_{xz}^{(0)} = 0, \quad z = z_b^{(0)}, \tag{A16}$$

$$\partial_x z_b^{(0)}\upsilon^{(0)}e_{xz}^{(0)} - \upsilon^{(0)}e_{zz}^{(0)} + \Gamma P^{(0)} = -(\rho_w/\rho_i)\Gamma z_b^{(0)}, \quad z = z_b^{(0)}. \tag{A17}$$

https://doi.org/10.3189/S002214300000914X Published online by Cambridge University Press

The zero-order solutions can be obtained immediately by integrating Equations (A12) and (A13) subject to the boundary conditions (A14)–(A17):

$$e_{xz}^{(0)} = 0, \tag{A18}$$

$$p^{(0)} = (z_s^{(0)} - z) + (\upsilon^{(0)}/\Gamma)e_{zz}^{(0)}, \tag{A19}$$

$$z_b^{(0)} = \rho_i/(\rho_i - \rho_w)z_s^{(0)}. \tag{A20}$$

The above solutions indicate that: (i) vertical shear in the ice column is negligible, (ii) pressure increases linearly with depth, and (iii) the ice shelf floats in local hydrostatic equilibrium.

A sub-set of the first-order approximations to Equations (A4)–(A9) (for the x-component of forces) describes how the zero-order strain-rate $e_{xx}^{(0)} = -e_{zz}^{(0)}$ varies with $H^{(0)} = z_s^{(0)} - z_b^{(0)}$:

$$\partial_z \upsilon^{(0)} e_{xz}^{(1)} = \Gamma \partial_x p^{(0)} - \partial_x(\upsilon^{(0)} e_{xx}^{(0)}), \qquad z_b^{(0)} < x < z_s^{(0)}, \tag{A21}$$

$$\upsilon^{(0)} e_{xz}^{(1)} = \partial_x z_s^{(0)}(\upsilon^{(0)} e_{xx}^{(0)} - \Gamma p^{(0)}), \quad z = z_s^{(0)}, \tag{A22}$$

$$\upsilon^{(0)} e_{xz}^{(1)} = \partial_x z_b^{(0)}(\upsilon^{(0)} e_{xx}^{(0)} - \Gamma p^{(0)} - \rho_w/\rho_i \Gamma z_b^{(0)}, \quad z = z_b^{(0)}. \tag{A23}$$

Integration of Equation (A21) over z using boundary conditions (A22) and (A23), followed by integration of the result over x (assuming that $e_{xx}^{(0)} \to 0$ as $H^{(0)} \to 0$, and that Γ, ρ_w, and ρ_i are independent of x) gives

$$\upsilon^{z(0)} e_{xx}^{(0)} = \tfrac{1}{4}\Gamma(1 - \rho_i/\rho_w)H^{(0)} \tag{A24}$$

where

$$\upsilon^{z(0)} = \int_{z_b^{(0)}}^{z_s^{(0)}} B(z')\,dz' / (e_{xx}^{(0)})^{1-1/n}. \tag{A25}$$

Substitution of Equation (A25) into (A24) gives Equation (2) of the main text:

$$e_{xx}^{(0)} = \partial_x U = A^n H^n \tag{A26}$$

where

$$A = \tfrac{1}{4}(\Gamma/B^z)(1 - \rho_i/\rho_w) \tag{A27}$$

is a non-dimensional parameter that measures the ratio of the gravitationally driven spreading stress to the stress required to deform the ice shelf at the far-field strain-rate scale U_0/L_0.

We have now shown that large-scale ice-flow is predominantly depth-independent and satisfies a simple relation between horizontal spreading and local thickness. To determine how this large-scale flow is forced at the ice-stream outlet, we next examine the small-scale effects expected close to the grounding line.

NEAR-FIELD DYNAMICS

To facilitate an exact solution of the stress-equilibrium equations that have been scaled to represent conditions close to the grounding line, we make two simplifications: (i) we assume υ to be a constant (chosen to correspond with some unspecified reference stress), and (ii) we replace the dynamic boundary conditions specifying stress at z_s and z_b (Equations (A7) and (A9)) with kinematic constraints motivated by the large-scale nature of the surface and basal topography. Equations (A4)–(A9) and the mass continuity constraint thus are written in terms of near-field flow variables only (subscripts n are dropped for clarity):

$$-(2\Gamma/\upsilon)\partial_\zeta p + \nabla^2 u = 0, \qquad z_s > z > z_b, \tag{A28}$$

$$-(2\Gamma/\upsilon)(\partial_z p + 1) + \nabla^2 w = 0, \qquad z_s > z > z_b, \tag{A29}$$

$$\partial_z u = 0, \qquad z = z_s, z_b, \tag{A30}$$

$$w = 0, \qquad z = z_s, z_b, \tag{A31}$$

$$\partial_\zeta u + \partial_z w = 0, \qquad z_s > z > z_b \tag{A32}$$

where $\nabla^2 = \partial_\zeta^2 + \partial_z^2$. The eigensolutions of Equations (A28)–(A32) are:

$$u_n = C_n \cos[k_n(z - z_s)]e^{-k_n\zeta}, \tag{A33}$$

$$w_n = C_n \sin[k_n(z - z_s)]e^{-k_n\zeta}, \tag{A34}$$

$$p = z_s - z \tag{A35}$$

where the eigenvalue k_n is given by

$$k_n = n\pi/(z_s - z_b) \tag{A36}$$

where $n = 0, 1, 2, \ldots$. The key feature of these eigensolutions is that all except that associated with the $k_0 = 0$ eigenvalue exhibit exponential decay as $\zeta \to \infty$. The $k_0 = 0$ eigensolution thus represents the part of the near-field flow that forces the far-field flow. This special eigensolution exhibits zero vertical shear and is thus compatible with far-field dynamics.

To satisfy an arbitrary ice-stream influx condition (e.g. $u(\zeta = 0, z) = (z_b - z)^2$), we simply express the prescribed influx as a linear combination of the eigensolutions described above. The $k_0 = 0$ contribution of the prescribed influx, for example, is simply the vertical average of the horizontal flow at the grounding line. As indicated by the exponential factors in the eigensolutions, all terms except that associated with $k_0 = 0$ are winnowed within a narrow region of the grounding line. In fact, modes with greater vertical structure and higher values of k_n decay more quickly than modes with grave vertical structure.

SUMMARY

We have shown that large-scale ice-shelf flow (the far-field flow) is forced by depth-averaged horizontal flux at the grounding line, even if the vertical profile of the horizontal flux deviates significantly from this average. Vertical structure not allowed by simple conditions prevalent down-stream decays exponentially over horizontal distances comparable to the ice thickness. This behavior is similar to other systems in which conditions far from boundaries exhibit intrinsically simple flow such as: shallow-water waves forced by complicated wave makers (see Yih, 1969, p. 195), or the flow of a homogeneous, rotating fluid forced by horizontal injections at lateral boundaries (Barcilon, 1967). The analytic approach we use to determine the behavior of the near-field solution requires linearity. Numerical solutions of the full non-linear near-field behavior (Herterich, 1987) confirm the behavior we deduce here.

MS. received 11 August 1987 and in revised form 16 November 1987